Journal of Building Engineering Event Based Approach for Modeling Indoor Airflow Patterns --Manuscript Draft--

Manuscript Number:				
Article Type:	Research Paper			
Section/Category:	HVAC systems			
Keywords:	built environment airflow transient flow simulation indoor air quality			
Corresponding Author:	Ehsan Mousavi, Ph.D. Clemson University Clemson, SC UNITED STATES			
First Author:	Ehsan Mousavi, Ph.D.			
Order of Authors:	Ehsan Mousavi, Ph.D.			
	Arup Bhattacharya			
Abstract:	People spend more than 75% of their time indoors, where the quality of indoor air affects the productivity, efficiency, and well-being of occupants. One of the oldest challenges in building construction is designing a ventilation system that ensures optimum indoor air quality. Acceptable indoor air should provide thermal comfort and minimize human exposure to contamination. Characterizing these two elements requires information on both heat/mass transfer in the microenvironment and the time-specific activity of individuals who move among these microenvironments. While researchers have utilized simulation tools to investigate this complex human-environment interaction, current numerical techniques severely limit the simulations to overly simplified, unrealistic scenarios. To address these issues, this paper proposes a new and innovative approach called the event-based modeling (EBM) to simulate airflow patterns for realistic human-environment interactions. EBM can provide an accurate approximation to simulate the patterns of air movement in indoor environments. EBM can also provide a path to simulate complex, random human-environment interactions that are pragmatically impossible to solve by current approaches. This paper formulates and evaluates this novel approach, and then validates it via a simple case of a door opening and human walking.			
Suggested Reviewers:	John Zhai John.Zhai@colorado.edu expert in the field Atila Novoselac atila@mail.utexas.edu Expert in the field			
Opposed Reviewers:				



Dear Drs. de Bitro, LaFave, and Yao,

November, 19, 2020

A paper titled 'Event Based Approach for Modeling Indoor Airflow Patterns' has been submitted to the Journal of Building Engineering. This paper highlights the results of a novel simulation approach to model the transient effects of human-environment interactions with indoor airflow patterns. The proposed approach, Event-based modeling (EBM) is a new methodology developed and tested via a series of experiments, conducted in a controlled environment under various walking schemes and flow conditions.

DEPARTMENT OF CONSTRUCTION SCIENCE AND MANAGEMENT

Clemson University 2-134 Lee Hall Clemson, SC 29634-0507

P (864) 656-6739 clemson.edu/caah/csm

We define the problem, formulate it, and propose three solutions. These three methods are all tested and evaluated via experimental data. To that end, we've categorized our experimental dataset into a training set and a test set. EBM uses the data available in the training set to approximate cases within the test set.

To the best of the authors' knowledge, this paper is unique and contribute to the state-of-the-art at least in three ways:

- 1. It provides a new approach to model transient airflow patterns indoors.
- 2. The proposed model requires significantly less amount of time and computationall capabilities, which makes it a favorable choice for intricate indoor air modeling
- 3. It tests the methods and validates the outcomes via actual experimental data.

As the corresponding author of this research, I attest to its originality and accuracy and do hereby certify that the author(s) have no known conflict of interest and are in full compliance with the submission declaration.

With Warm Regards,

Ehsan S. Mousavi* Ph.D.

Assistant Professor, Department of Construction Science and Management

Clemson University

2-132 Lee Hall, Clemson, SC, 29634

(cell) 402.314.7726

ehsan.mousavi@unl.edu (corresponding author)

Highlights

- 1. Event based modeling is a novel approach to simulate transient airflow in buildings
- 2. EBM uses past stored data to predict similar future interactions
- 3. 360 tests were conducted on transient door opening and human walking events
- 4. Results show an average prediction error of less than 4% for the proposed method
- 5. Fast and accurate airflow prediction enables efficient indoor air quality assessments

Event Based Approach for Modeling Indoor Airflow Patterns

Ehsan Mousavi*

Department of Construction Science and Management, 2-132 Lee Hall, Clemson University, mousavi@clemson.edu

Arup Bhattacharya

Department of Construction Science and Management, Clemson University, arupb@clemson.edu

Abstract

People spend more than 75% of their time indoors, where the quality of indoor air affects the productivity, efficiency, and well-being of occupants. One of the oldest challenges in building construction is designing a ventilation system that ensures optimum indoor air quality. Acceptable indoor air should provide thermal comfort and minimize human exposure to contamination. Characterizing these two elements requires information on both heat/mass transfer in the microenvironment and the time-specific activity of individuals who move among these microenvironments. While researchers have utilized simulation tools to investigate this complex human-environment interaction, current numerical techniques severely limit the simulations to overly simplified, unrealistic scenarios. To address these issues, this paper proposes a new and innovative approach called the event-based modeling (EBM) to simulate airflow patterns for realistic human-environment interactions. EBM can provide an accurate approximation to simulate the patterns of air movement in indoor environments. EBM can also provide a path to simulate complex, random human-environment interactions that are pragmatically impossible to solve by current approaches. This paper formulates and evaluates this novel approach, and then validates it via a simple case of a door opening and human walking.

keywords: built environment, airflow, transient flow, simulation, air quality.

1 Introduction

Indoor air quality (IAQ) is a major environmental health issue, as we spend up to 90% of our time indoors [1]. People, occupant activities, building material, and even outdoor air emit pollutants into indoor air. These emissions vary among buildings by contaminant type, as well as temporally and spatially within the building [2]. The engineering solution has long been dilution/removal of the contaminants by introducing fresh air through the ventilation system. Hence, inadequate ventilation rates have been

historically associated with certain health outcomes and adverse air quality perceptions [3, 4].

The outbreak of COVID-19 has rejuvenated the research efforts in airborne contamination control. This topic has received renewed interest from the entire built environment research community in light of ample evidence that SARS-CoV-2 can be airborne. Morawska and Cao (2020) have argued that it is logical to consider the possibility of airborne transmission of the novel Coronavirus, as its closest known relative, SARS-CoV-1 was found to be passive [5]. This hypothesis have been supported by other scientists who argued in favor of considering airborne route as a significant transmission mechanism for COVID-19 [6]. On-field experiments in the Wuhan Hospitals, China have also conclusively shown that SARS-CoV-2 is capable of staying afloat in the air for traveling up to 10m [7]. Hence, from the public health perspective, it is crucial that the ventilation system should be designed to mitigate/contain airborne dispersal of pathogens, especially in healthcare facilities.

The association between proper ventilation and health outcomes has also been studied in built environments other than healthcare facilities. Several studies of single- and multi-family homes have found a direct association between lack of fresh air and health symptoms for asthma, bronchial obstruction, and eczema [8, 9, 10]. Also, Milton and colleagues (1998) found that short-term sick leaves were reduced by increasing the amount of fresh air [11]. In all of these papers, only ventilation rate was used as a suggestive measure of IAQ level. When ventilation rate is studied as the indicator for IAQ, the current design paradigm considers only the steady-state aspect of the flow. Bhattacharya et al. (2020, 2021) have conducted experiments in a cleanroom and a controlled environment chamber to demonstrate the impacts occupant-environment interactions have on the steady-state airflow fields [12, 13, 14].

Occupant-introduced perturbations, opening and closing of doors, and walking movements being two of the most common disturbances, break down the steady-state conditions that to a transient flow system. Several studies have discussed how these perturbations affect steady-state indoor airflow. Josephson and Gombert (1998) studied the outbreak of airborne nosocomial varicella and showed that the increased number of patients with the disease when the nursing station was placed adjacent to the patient room because of the increased movement of indoor occupants that aided in the dispersion of the contaminants [15]. With the advancement in computing and more robust experimental designs, studying occupant intervention has become more accessible in recent times. Numerical simulation of an isolation room by Shih et al. (2007) showed the effects and distribution of flow fields under the influence of human movement and door operation [16].

Door opening adversely impacts spaces with pressure differentials as it disrupts the isolation condition

[17, 18]. A study by Gustavsson (2010) revealed the creation of vortices due to door opening [19]. Frequent door openings were related to the interruption, potentially reversing differential pressure related to an increased transmission rate [17]. In that study by Mousavi et al. (2016) shown through a numerical simulation study that operating the isolation room door could transport 5% of the isolation room air to a cleaner environment, and the speed of door operation is inversely proportional to exchange volume across the opening [17]. Existing research suggests the frequency of door opening in an operating room, ranging from 37 to 40 times [20], during a surgical intervention depends on the type of procedure [21, 22] for obtaining supplies, paperwork, shift change, and communication [21]. Several studies concluded that door motion is a plausible mechanism for mass transfer through volumetric air exchange [23, 24, 25, 26, 27]. Hang et al. (2015), through a numerical simulation, demonstrated that the door opening results in the volumetric exchange of air at the two sides of the door, effectively introducing unwanted particles on either side [28].

The generation of vortices at the door tip in swinging motion and propagation of those vortices through the flow field in the room was indicated by Eames et al. (2009) in their experiment involving measurements of dye concentrations in a mock-up room [29]. An experimental study conducted in office rooms and laboratories showed that with a more extended period of keeping the door ajar, the swept volume is close to equal to that of exchange volume [30]. The incoming traffic movement to a chamber followed by a door opening has higher impacts on the door movement generated flow field, as demonstrated through an experimental study by Villafruela et al. (2016) [31]. Lin et al. (2007) demonstrated that the opening of doors affects the pressurization scheme [32]. Using 3-dimensional velocity measurements near the door, Papakonstantis and colleagues (2018) demonstrated the movement of flow vectors while opening and closing the door. They explained the advection of flow vortex along the wall during the opening [33]. In a two-dimensional numerical simulation study of a door opening, Bhattacharya et al. (2020) showed that the door opening and closing movement has profound impacts on the velocity profiles and the direction of streamlines [34]. As demonstrated through that study, the region close to the door tip was associated with the highest velocity magnitude during the door motion. It was also discussed that the flow field recorded a higher speed during the closing motion compared to the opening. 10% of the total air change could escape from opening a swing door for 5s, as demonstrated by Bhattacharva et al. (2021) [13]. By the early 1980s, scientists found shreds of evidence of the interaction between the flow fields and personnel movement. The indoor walking motion of occupants having an impact on the spread of particles was predicted by Leclair et al. (1980) [35]. Several studies examined the change in flow velocity due

to the movements of objects in a variety of settings [36, 37, 38]. Most of these earlier studies employed surrogate methods of measurements (e.g., tracer gas method, scaled experiments, etc.). Poussou et al. (2010) demonstrated the distribution of air vortices, and consequently the contaminants, in an airliner cabin resulting from the interaction of the human movement generated wakes and the existing flow fields [39]. Luo et al. (2018) conducted computational fluid dynamics (CFD) simulations, validated by scaled experiments to show the downward flow of airflow vortices before getting dispersed horizontally near floor level that follows a moving human body [40]. The author also pointed out that the rate of dispersion was related to the movement speed. Mazumdar et al. (2010) replicated a hospital inpatient ward through a simulation study. They established that contaminants are moved through the wakes behind moving objects (e.g., people, equipment, etc.) [41]. Similarly, the numerical simulation study of a laminar airflow orthopedic surgery room by Brohus et al. (2006) established that the flow profiles, both local (in close vicinity of the moving body) and overall (for the whole room), are severely impacted by movements of the healthcare workers. Periodic movements after near-constant intervals were behind the origin of complex turbulent flow inside the room, reducing the efficiency of the ventilation system [42].

Han et al. (2015) examined the aerodynamics of airflow patterns and contaminant transport under the influence of indoor movements in settings apart from healthcare facilities [43]. The movement of occupants generates wakes that follows the movement, and those wakes disrupt the normal flow properties, leading to contaminant dispersion [44]. Scaled experiments of indoor airflow were conducted using waterfilled 3-D models to study the effects of external perturbations, as Rouaud and team (2004) conceived that full-scale experiments were not feasible [45]. Cheng and Lin (2016) found the "blockage effect" that restricts the air to flow without hindrances, as they substituted the human subject by using manikins to investigate how a moving human body interacted under stratum ventilation [46]. Choi et al. (2012) examined the dispersal of airborne particles due to occupant movement from a contaminated room to a clean one, connected by a vestibule using large-eddy simulations. Their findings indicated that motion-induced wakes were behind the cross-contamination by particles from one compartment to another [47]. Han et al. (2015) mathematically modeled the in-flight spread of airborne infectious disease through likelihood analysis, using an Eulerian-Lagrangian approach [43]. The results provided evidence to corroborate previous findings of human movement disturbing air distribution and provided insight that enhanced air mixing was evident that aided the transfer of particles along the movement direction. Tao et al. (2017) suggested that the change in momentum of the airflow that follows walking motion helps distribute the particles. They demonstrated the lingering effects of walk that continue to influence the flow fields even

after movement is ceased [48]. A realistic CFD simulation of a healthcare worker's movement involving swinging arms and legs by Hang et al. (2014) in an isolation room showed a complex air mixing that generated wakes up to 6 m long and diminished after 30-60 seconds after the termination of movement [49].

In general, however, experimental assessment of IAQ is difficult. Measurement of IAQ is limited by the number and location of sensors. Therefore, a full spatial/temporal analysis of IAQ is unfeasible under practical conditions and tends to be very expensive. Therefore, researchers have utilized computer models. In particular, computational fluid dynamics (CFD) models have been evolved to simulate airflow patterns (carrier-domain) and contaminant transport in buildings. Two accepted approaches are used to model the motion of a second species in a carrier domain: the Eulerian and Lagrangian methods. The Eulerian method treats the contamination as a continuum within the carrier domain, solves the fundamental equations for the new species, and considers the interaction between species. This method, however, is established for environments in which the second species' concentration is sufficiently large to create a continuum [50, 51]. Alternatively, the Lagrangian method treats contaminants as solid, non-deformable entities whose motion is determined by the forces exerted on them [52]. The Lagrangian method tracks particles by solving the following ordinary differential equation:

$$\frac{d\vec{u_p}}{dt} = F_D(\vec{u} - \vec{u_p}) + \frac{\vec{g}(\rho_p - \rho)}{\rho_p} + \vec{n}(t) + \vec{F_L} + \vec{F}$$
(1)

where the only unknowns are particle velocities. \vec{u} and $\vec{u_p}$ are air and particle velocity, respectively. The first term on the right-hand side of the equation is the drag force, F_D , given by:

$$F_D = \frac{18\mu}{\rho_p d_p^2} \frac{C_D Re}{24} \tag{2}$$

where ρ_p and d_p are the particle density and diameter, respectively; ρ and μ are air density and viscosity; Re is the Reynolds number, and C_D is the drag coefficient defined by Hinds [53]. The second term is associated with gravity and buoyancy. n(t) and F_L are the Brownian and Saffman's lift force, respectively, and the last term represents other forces such as the virtual mass and pressure gradient forces, if present [54]. For a known air velocity field (\vec{u}) , particle velocity will become the only unknown of an ordinary differential equation (Eq. (1)). Particle trajectories are computed with the following equation

$$\vec{u_p} = \frac{d_{\vec{x}_p}}{d_t} \tag{3}$$

where \vec{x}_p is the particle position vector in the domain. Thus, knowledge about indoor air patterns will result in real-time modeling of contaminant spread as a function of time. In this scheme, complexity, size, and human-building interactions in the model will become irrelevant, as long as the velocity field is known. Hence, the event-based modeling approach focuses on airflow patterns as necessary information for IAQ assessments. The main goal of this paper is to propose a **new approximation methodology** for transient indoor air patterns modeling. This method, referred to as the event-based modeling (EBM) approach, proposes that repetitive human-environment interactions (e.g., walking) could be modeled once and be used multiple times. This approach can eliminate parallel modeling of the same phenomena. It must be noted that EBM does not require the events to be sequential. They can be simultaneous and/or have overlaps.

2 Core Idea

The core idea of EBM is that every interaction between a subject and its surroundings can be broken down into a series of events. Consider a simple scenario of an office with a person standing 2m away from the door. Then this person decides to move toward the door and leave the room. By focusing on what drives the fluid flow in this scenario, two major causes are identified: 1) steady events: those that are constant in time, such as a constant air volume ventilation system or a ceiling fan running with a constant angular velocity; and 2) transient events: those that change with time. Modeling of the first group is less expensive and has been extensively utilized. EBM specifically targets the latter category. In the above example, two main transient events are identified: walking and door opening. The EBM approach develops walking and door opening models separately. The walking model simulates the movement of the human body in quiescent air. The model is run until air velocities approach zero. Experiments show that for a 2m walk at 1m/s speed, the velocity field reaches $\pm 0.03m/s$ everywhere in 20 seconds [14]. While a steady model describes airflow before the person decides to move, the 20s walking model can be superposed on the steady model to describe airflow. The same logic will be followed for door opening. Suppose that one intends to model the airflow in a room for one hour including the transient effect of the door opening. Previous efforts show that numerically simulating this work can take weeks if not months to complete due to small timesteps. For instance, Carneiro et al. reported that modeling one

door operation (14s) took about 168 hours [55]. In response, EBM proposes that instead of developing a transient model for the full duration of interest, transient events (i.e., door opening and human walking) can be modeled separately and the results be stored. Developing models for each event is computationally intensive and could take long times to converge. However, these models will be run once and used multiple times. Calling out a stored result is much less expensive than running the model each time. The EBM approach uses the existing model for an event and superposes the stored results to the current field. The true challenge of EBM then becomes how to methodically define superposition in this case. For an inviscid flow where the Navier-Stokes equation simplifies to a linear partial differential equation (PDE), the superposition can simply become an addition. For more complex, realistic flow fields, however, one has to rigorously define superposition.

3 EBM Definition of Superposition

Let's consider a simple transient event that is quite frequent in the indoor environment: door operation. Also, let's assume that the door operates every time with the same angular velocity and the same opening-closure cycle and other boundary conditions. As stated in the previous section, EBM proposes that this event can be revived from a set of known cases with available solutions. Numerically speaking, any subsequent repetitions of door opening in a constant boundary conditions environment (i.e., the same room) would be identical to previous events, with a different initial condition. Let's denote the velocity field of due to a new event (E_i) by $\vec{U}_i(\vec{x},t)$ with an initial condition of IC_i . Note that IC_i is known as it is equivalent to the latest state of the system before event E_i occurs. EBM Assumes that the velocity field due to a new case can be approximated by a function $f_i(\vec{U}^*(\vec{x},t),IC_i)$ where \vec{U}^* is a glossary of solutions of the same event under different initial conditions. The true contribution of EBM relies on proposing a method to approximate f. Without loss of generality, the N-S equation can be written in 2-D where \vec{u} and \vec{v} are the x- and y- direction velocity magnitudes.

$$\rho \frac{\partial \vec{u}}{\partial t} + \vec{u} \frac{\partial \vec{u}}{\partial x} + \vec{v} \frac{\partial \vec{u}}{\partial y} = \mu \left(\frac{\partial^2 \vec{u}}{\partial x^2} + \frac{\partial^2 \vec{u}}{\partial y^2} \right)$$

$$\rho \frac{\partial \vec{v}}{\partial t} + \vec{u} \frac{\partial \vec{v}}{\partial x} + \vec{v} \frac{\partial \vec{v}}{\partial y} = \mu \left(\frac{\partial^2 \vec{v}}{\partial x^2} + \frac{\partial^2 \vec{v}}{\partial y^2} \right)$$

$$(4)$$

Using a standard numerical approach (e.g., the explicit central difference), it can be shown that spatial

velocities for a particular timestep can be written as a linear combination of spatial magnitudes from the previous timestep. In that sense, the problem is Markovian, i.e., the current state of the system is sufficient to simulate its future. Hence, the matrix \mathbf{X}^* is defined from each $\vec{U}^*(\vec{x},t)$ where rows of \mathbf{X}^* represent velocity magnitudes at n discrete spatial point and columns provide data for m time step. For one known case of $\vec{U}_0(\vec{x},t)$ we will have:

$$\mathbf{X}_0 = [\vec{U}_0(\vec{x}, t_0), \vec{U}_0(\vec{x}, t_1) \dots, \vec{U}_0(\vec{x}, t_m)] \in \mathbb{R}^{n \times m}$$
(5)

Solely for simplicity, let us replace the notation $\vec{U}_0(\vec{x}, t_i)$ with u^i . In this construct, an identifier α can be defined to linearly approximate u^{i+1} from u^i .

$$(u^{i+1})_{1\times n} = (u^i)_{1\times n} \times \alpha^i_{n\times n}$$

$$\alpha^i = (u^i)^{p_{-1}} \times u^{i+1}$$
(6)

Note that in Equation (6), the p_{-1} is the pseudo-inverse operator. With this approach, a time-variable α ($\in \mathbb{R}^{n \times n \times m-1}$) can be found for each known case that would make possible prediction at each timestep based on the previous timestep. Let's assume that a total of K previous cases with known solutions are available, i.e., \mathbf{X}_1 to \mathbf{X}_K . Hence, α can be calculated and stored for each case. To predict a new case (i.e., \mathbf{X}_{new}), one only needs to approximate the α_{new} and use that to predict velocity magnitudes beyond the initial condition. Several approaches could be perceived to reconstruct α_{new} from a set of known α 's. In this paper we propose three approaches, test each approach via a theoretical framework and experimental observations.

3.1 Weighted Average of Known Cases

Perhaps the very first approach to reconstruct α_{new} is the estimate it as some weighted average of $\alpha_1 \dots \alpha_K$.

$$\alpha_{new} = \sum_{i=1}^{K} \alpha_i \zeta_i \tag{7}$$

Where $\zeta_i's$ are linear coefficients that demonstrate the contribution of each case to α_{new} . One way to estimate ζ_i is by projecting the initial condition of the new case IC_{new} on those of the existing cases. Therefore,

$$IC_{new} = \sum_{i=1}^{K} IC_i \zeta_i \tag{8}$$

Note that in practice, Equation (8) is converted to a minimization problem where ζ_i is estimated to minimize the difference between the left and right hands side of Equation (8). To avoid unreasonably large ζ values, a constraint could be added to force the sum of these coefficient equal to unity.

$$min(IC_{new} - \sum_{i=1}^{K} IC_i\zeta_i)$$

$$S.t. \sum_{i=1}^{K} \zeta_i = 1$$
(9)

Theoretically, this approach assumes that the α and the initial condition (IC) of the system covary linearly. However, Equation (6) shows that α is calculated from the pseudo-inverse of IC, therefore the linearity assumption is under serious question. The experimental results, presented in the results section, substantiate this theoretical conflict.

3.2 Closest Case

One special case for the weighted average approach is when the number of known cases (i.e., K) is equal to the number spatial points (n), in which case, Equation (8) will become a determined algebraic system and ζ has an exact solution. However, this approach is essentially data-fitting, where spatial values of the IC_{new} are fitted by a linear combinations of a known case. Therefore, the solution for ζ will become sensitive to the IC of the known cases, and outlier cases can produce great 'noise' to the prediction (see the results section). A reasonable variation of the weighted average approach is only use a subset of the known cases closest to the new case. In this approach, IC_{new} will be first compared the existing cases, and a predetermined number of close case will be chosen to predict α_{new} . This approach can have a great theoretical promise. Suppose that there are an infinite number of known cases. Then there will exist a known case that is identical to the new case. Then using Equation (6), one can find the exact velocity magnitudes. Similarly, the closest case approach can be reduced to choosing the closest known case for prediction. Algorithm (1) depicts the mechanics of this approach, and the results section presents our experimental findings about this approach.

3.3 Dynamic Closest Case

As alluded to earlier, the closest case approach returns the exact solution as the number of known cases approaches infinity. Yet, in the absence of sufficient number of known cases, one perceived improvement

Algorithm 1 EBM's Closest Case Approach

```
Let <\mathbf{X}_1,\ldots,\mathbf{X}_K> be the K known Cases

Let IC_{new} be the initial condition of the new case and < IC_1,\ldots,IC_K> be the initial conditions of the known cases

for q=1,2,\ldots,K do

d_q=norm(IC_{new}-IC_q)

end for

Q=Index(min(d)) Determine the closest case

\alpha_{new}\approx\alpha_Q

for i=1,2,\ldots,m do

(u_{new}^i)=(u_{new}^{i-1})\times\alpha_{new}^i note that u^{i-1}=IC_{new} for i=1

end for
```

is to dynamically search for the 'closest case' at each timestep. That is, Algorithm (1) will be used to estimate the velocity magnitudes (u) only for the second timestep. In this approach, we aim to find, independently, the closest case at every timestep, meaning that at each iteration α_{new} could come from a different case. This could potentially result in smaller error. Experimental findings about this approach are offered in the results section.

4 Methods

The Center for Built Environment at the University of California, Berkeley has a controlled environment chamber, which was used to conduct experiments during Summer 2019. This 5.48m x 5.44m x 2.5m experiment facility, has a door of 1.98m x 0.98m at one corner (Figure 1). This chamber is equipped with an air conditioning system that can supply air at altering rates from the 0.3m x 0.3m diffuser mounted on the wall at a height of 0.3 m from the ceiling. The exhaust grilles were shut off during the experiments, and the excess air was exfiltrated through the gap around the door, creating different levels of positive pressure inside the chamber with respect to the corridor outside, depending on the air supply rate. Experiments were carried out based on two door movements and two walking movements under three different air supply rates inside the chamber (a) still air: where the ventilation system was shut off, (b) 0.5 ACH which is equivalent 70% fan where the ventilation system was throttled to supply air at 70% of the full capacity, and (c) 100% fan when the ventilation system was supplying air at maximum capacity. These flow regimes created the overall steady-state condition of the room prior to the transient events (i.e., door and human movements). Table 1 shows the the various experimental configurations, duration, and the number of repetitions.

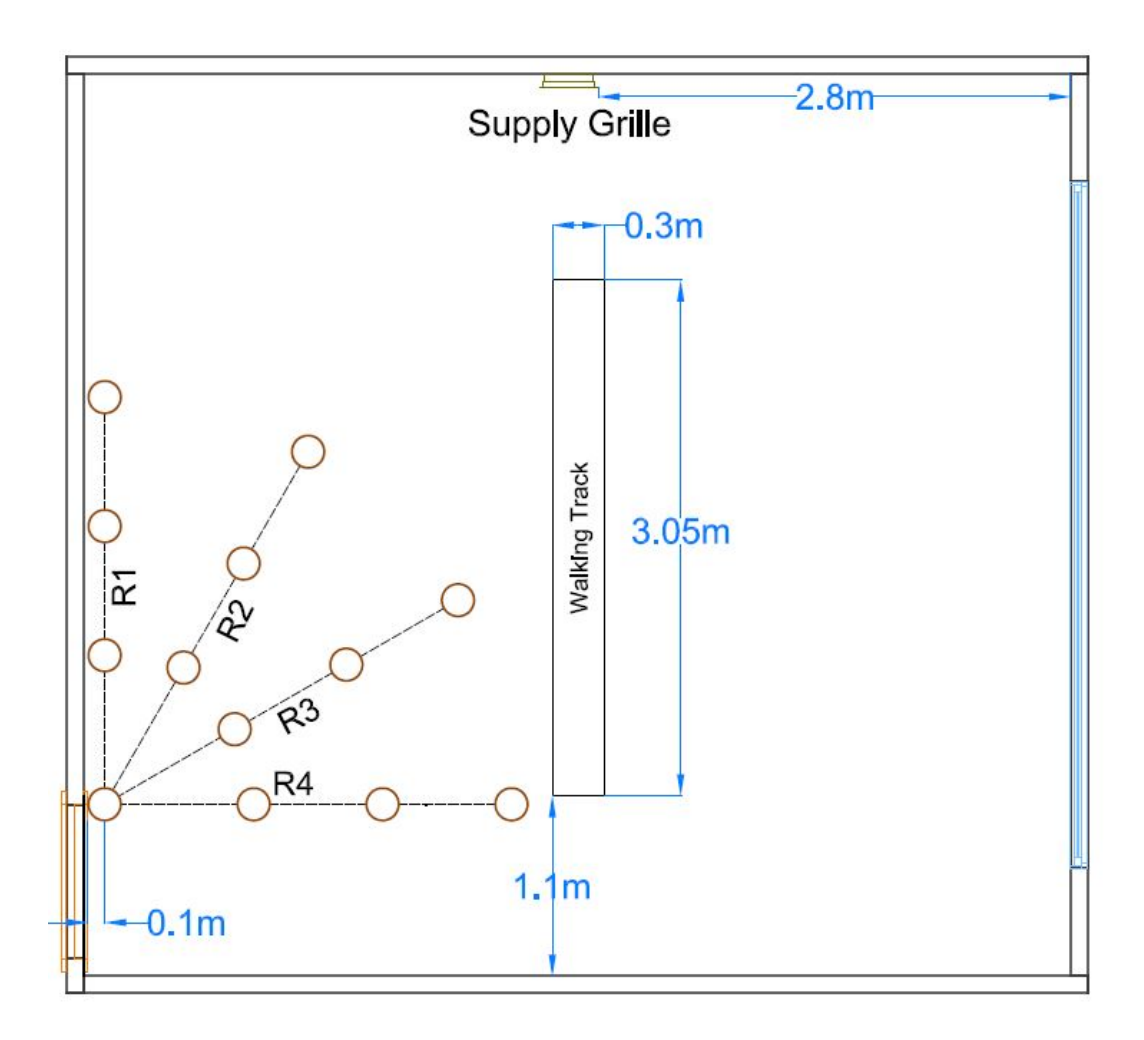


Figure 1: Experiment Setup: Arbitrary Rows (R1 through R4) of Sensor Arrangement for Door Opening Exercises (left) and The Walking Track (center)

4.1 Experiment Setup

To study the spatial/temporal effects of occupant movement on the indoor airflow fields, a series of walking experiments were conducted. A 3.04m long and 0.3m wide walking track was defined to control for inherent randomness of human walk. Sensors were placed at both sides of the track to measure air velocity. The occupant started the walk from the point which was 1.1m from the bottom wall in Figure 1. The tripod-mounted sensors were placed in six imaginary lines perpendicular to the walking track, with a distance of 0.61m between them. For walking once, the walking movement began at the starting point the track distance (3.04m) was covered in three seconds before coming to a standstill (walking speed = 1.02m/s). As the movement direction of the walking was towards the supply grille, this scenario was designated as the forward movement. During walking twice, the forward walk was completed in three seconds and after remaining stationary at the end of the walking track for one second, the backward

Table 1: Experimental Setup

No.	Event Details	Initial	Mean Duration	Duration of	Repetitions
		Condition	of Event	Data Collection	
1		Quiescent Air	$3.18 \text{ s } (\sigma = 0.27)$	60 (s)	30
2	Walking Once	$70\% \mathrm{Air}$	$3.20 \text{ s } (\sigma = 0.13)$	$60 \ (s)$	30
3		$100\%~\mathrm{Air}$	$3.09 \text{ s} \ (\sigma = 0.17)$	60 (s)	30
4		Quiescent Air	$7.18 \text{ s } (\sigma = 0.23)$	60 (s)	30
5	Walking Twice	$70\%~{ m Air}$	$7.01 \text{ s } (\sigma = 0.18)$	$60 \ (s)$	30
6		100% Air	$7.07 \text{ s } (\sigma = 0.14)$	$60 \ (s)$	30
7	Door Opening	Quiescent Air	$5.38 \text{ s } (\sigma = 0.21)$	60 (s)	30
8	Once	$70\% \mathrm{Air}$	$5.52 \text{ s } (\sigma = 0.82)$	60 (s)	30
9		$100\%~\mathrm{Air}$	$5.42 \text{ s} \ (\sigma = 0.39)$	60 (s)	30
10	Door Opening	Quiescent Air	$12.33 \ (\sigma = 1.14)$	60 (s)	30
11	Twice	$70\%~{ m Air}$	$12.49 \ (\sigma = 0.24)$	60 (s)	30
12		100% Air	$12.48 \ (\sigma = 0.19)$	60 (s)	30

movement was done for another 3 seconds to reach the start point and stop walking. Both of these walking exercises were repeated 30 times, for each of the three initial conditions. The time-averaged outputs of the omnidirectional sensing system for every test case was collected for 60 seconds which generated 30 data points for each of the 30 replications (Table 1).

To study the effects of opening and closing a swing door on the steady-state indoor airflow patterns, sensors were arranged in four imaginary radial lines, as depicted by R1 through R4 in Figure 1. For door opening and closing once, at the first second of every repetition of each experiment the swing door is opened in 2 seconds, held open for one second, and then closed in another 2 seconds. The total time for a complete cycle of door opening-closing was ~ 5 seconds. For door opening and closing twice, the first round of opening-closing of the swing door was identical to that of door opening once scenario. After that, the door was kept shut for two seconds before the door is opened and closed again as was done during the first cycle (2s opening, keeping open for 1s, and 2s closing). It took ~ 12 seconds for this scenario of door opening events. These two door opening movements were conducted for 30 times at each of the three flow rates, and data was collected for 60 seconds for each experiment (Table 1). It is to be noted that the door opening and the walking experiments were not conducted simultaneously - each set of experiment was carried out separately.

4.2 Velocity Sensing Instruments

AirDistSys 5000 manufactured by Sensor Electronic, Poland was used as omnidirectional hotwire anemometer, that measured the magnitude of air velocity. There are three principal components of these sensors - a transducer, a converter and a transmitter. SensoAnemo5100LSF is a transducer of 2mm diameter, with measurement speed range of 0.05 to 5 m/s, accuracy of 0.02 m/s or 1.5\%, directional sensitivity error for v> 2 m/s of 2.5% of the actual value. These sensors recorded one data point every two second. AirDistSys 5000 is designed for low speed velocity measurement at indoor conditions, and it has wide range of frequency response with high sensitivity. The transducer measures instantaneous mean air speed and standard deviation of air speed. The probes in all the sensors were connected to SensoDACon series 5400 converter allowing the conversion of a digital signal with Sensoanemo transducer to the analog signal of velocity as output which was recorded in the system through wireless connection using SensoBee transmitter and receiver. The use of these sensors have been validated through a number of studies sensors [56, 57, 58, 59, 60]. The collected data was randomly assigned to a training set (80%) and a test set (20%). The training data embodied the K existing cases and were used to estimate a new case from the test set. Next, the EBM approximation of the new cases was compared against the experimental findings to study the error of each EBM approximation approach (i.e., weighted average, closest case, and dynamic case)

4.3 Error Measurements

To check the accuracy of the estimated velocity using Algorithm (1), the predicted velocity field u_{new} is compared to a test case (u_{test}) . Next, the absolute error (e) was defined as the absolute value of the difference between the predicted velocity and the measured velocity at each of the n locations at every timestep.

$$e = |u_{new} - u_{test}| \in \mathbb{R}^{n \times m} \tag{10}$$

To normalize the error and make it a dimensionless index, Relative Error (ϵ) is calculated by dividing the absolute error (e) by the measured velocity matrix u_{test} . As both $e \in \mathbb{R}^{n \times m}$ and $u_{test} \in \mathbb{R}^{n \times m}$; mathematically, ϵ can be defined by:

$$\epsilon = \frac{e}{u_{test}} \in \mathbb{R}^{n \times m} \tag{11}$$

While studying e and ϵ made the most granular level of analysis, in some instances in this paper we only offered the mean spatial (i.e., row average) or temporal (i.e., column average) errors. Moreover, all

the individual error data $(n \times m)$ are visualized using statistical histograms. In this particular case, we used the algebraic value of $u_{new} - u_{test}$ instead of the absolute value.

5 Results and Discussions

5.1 Experimental Results

The experiments, listed in Table 1, were conducted to obtain spatio-temporal data of the magnitude of flow velocity to study how different events affected the velocity fields under three supply conditions. While an interested reader can refer to [14, 13] for detailed experimental results, below are some major experimental findings related to the EBM approximation method.

- 1. The transient events, the walking movement of an occupant, and the door opening-closing movements, affect the steady-state airflow significantly. The two walking events of walking along a straight line at a speed of 1.02 m/s result in distinguishable and prolonged alterations in the steady-state flow patterns. Identically, changes in the flow fields were observed following the door opening events.
- 2. The impacts of the transient movements diffuses substantially. In the absence of any subsequent occupant introduced disturbances, the changes in the velocity fields were found to have diminished. For all of the walking and door opening events, the velocity sensors logged the changes in the flow velocity with some lag, meaning the recorded time of a change in velocity was after a few seconds from the time when the air actually flew past the sensors. Hence, even though the door opening started at the first second, the increase in velocity was observed with a lag. The trend showed that after the movement was stopped, the velocity values at each of the sensor locations dropped quickly.
- 3. The changes in the airflow from these transient occupant interventions last for < 60s. The analyzed data from all four events showed that following the movement of the subject or the door, the velocity values increased for ~ 15 s before the changes started to wear off at the location of observation. Collecting data for 60s for event duration of 3s (walking once), 7s (walking twice), 5s (door opening once), and 12s (door opening twice) provided ample opportunity to track the change in airspeed after the movement had ceased. It was found that under the three different flow conditions, the changed values of air velocity subdued within ~ 35 seconds after the sensors started recording changes.

- 4. When the effects of transient movements subdue, the state of the flow in the chamber converges to the steady-state as it was before the introduction of the perturbation. For walking motions, the flow velocity values after 40 seconds from the start of walking were comparable to that of the background velocity, i.e., the velocity values before the perturbation was initiated. Similarly, for door opening, there were no observable fluctuations after second ~ 35 , which represents the steady-state condition in the room.
- 5. The resultant flow from a typical transient event changes with the initial flow condition. The changes in the flow patterns from occupant induced transient events significantly depend on the initial condition. With the increased supply rate, the effects from human interventions subdued quicker and the changes in the velocity values were also larger when compared to the quiescent air case. The second cycle for walking twice and door opening twice happened with an initial condition of the residual motion from the first cycle. Hence, the turbulent interaction resulted in an increased velocity value for the events with a repetition (walking twice and door opening twice), compared to the single events (walking once and door opening once).

5.2 Assessment of EBM

To compute the new case and compare with the test case to determine the accuracy of the method, the data collected through the experiments are divided into training and testing sets. As explained in the method section, the weighted average approach to EBM is sensitive to the data used to approximate the α_{new} , as including every set of data introduces noise to the calculation, since in this approach every set of data in the training set contributes to the α_{new} in terms of the weight. Moreover, as the weighted average approach compares the initial condition of the test case and the training data, it would not be able to capture the difference in velocity magnitudes at later timesteps and would skew the approximation. For example, the velocity field obtained from door opening twice would be different from the velocity field obtained from door opening once, and computing a new case of door opening once from a dataset that includes both door opening once and twice data, would result in a poor estimate when using the weighted average approach. Hence, for the weighted average calculation, the obtained data was sorted into four distinct sets for the four specific events - door opening once, door opening twice, walking once, and walking twice, such that the dataset would only contain the specific event related information. Each of these four datasets had 90 sets of velocity fields, 30 for each of the three inlet airflow rate. Each of these 90 velocity matrices were divided into training and testing sets, where the 80% of the data (72 out

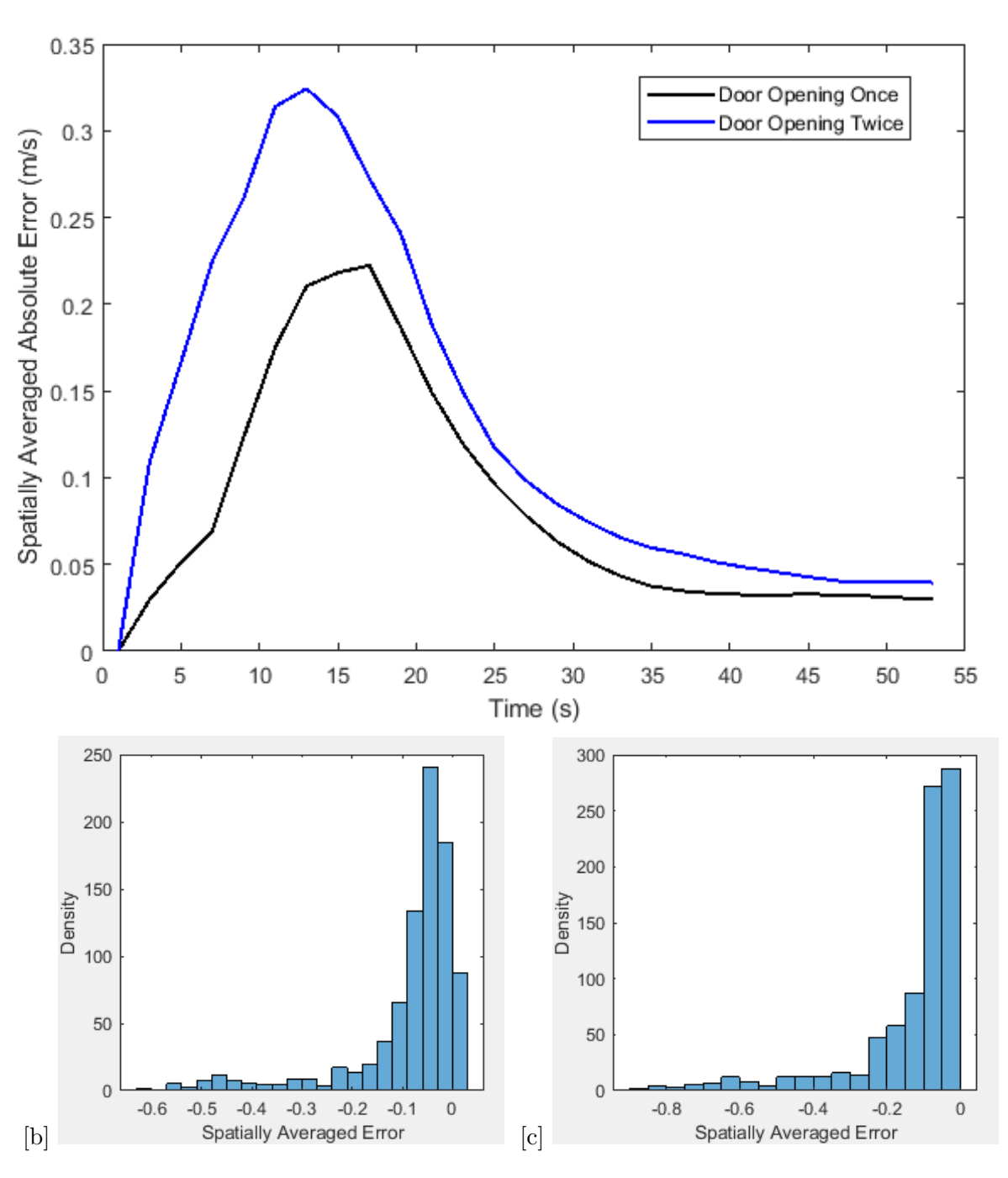
of 90) were randomly selected for training and remaining 18 sets of the data were kept for testing the approximation.

As the other two methods, closest case approach and dynamic closest case approach, compare the new case to the training set and find the closest velocity vector in the training set, the data only needed to be sorted for type of event, i.e., separate databases were created for door opening that had both door opening once and twice data, and for walking which also contained both walking once and walking twice data. That way, 180 sets of data were available for both types of interventions. In each case, 80% of the data were randomly chosen to form the training dataset and the testing dataset comprised the remaining 20% of the total data. This way, the known cases used for the approximation are a subset of the training set, whereas the u_{test} used to check the accuracy of the approximated new case is a subset of the testing set.

5.2.1 Weighted Average Approach

As explained, the approximation using the weighted average approach was done separately for four different events, namely door opening once, door opening twice, walking once, and walking twice. For each of these events, ζ_i 's were computed by solving the minimization problem offered in Equation (9). These ζ_i 's were then used to approximate α_{new} using Equation 7. Using the Initial Condition and this α_{new} , the new case is predicted and compared to a specific case from the test database. For simplicity and succinctness, the results of approximating one new case for door opening once and twice are discussed.

The spatially averaged absolute error (\bar{E}) when approximating a new case of door opening once and another new case for door opening twice are shown in Figure 2. It is evident that approximating the velocity fields using this approach results in a maximum of 22% and 32% error for door opening once and twice events, respectively. The highest errors are associated to the locations in the proximity of boundaries, i.e., walls and the moving edge of the door. Temporally, the higher errors are correlated to the door movement time. As the sensors recorded velocity values with some lags, Figure 2 shows an increasing trend in the error until ~ 17 seconds. This graph also demonstrates that computing for the door opening twice events results in a higher error compared to approximating for door opening once event. This could probably be attributed to the increased complexity of the velocity field resulted from subsequent door movements compared to opening and closing the door once. The distribution of spatially averaged errors when approximating new cases for both door opening once and twice shows that the error distribution is a left skewed, non-parametric distribution. Perhaps the small size of training samples as



[a]

Figure 2: Error from Door Opening Events - Weighted Average Approach: [a] Comparoison of Temporal Trend - Door Opening Once and Twice, [b] Error Distribution - Door Opening Once, and [c] Error Distribution - Door Opening Twice

well as computing the α_{new} as a linear combination of known α 's when known α 's are computed using pseudo-inverse, are contributing to the large errors.

5.2.2 Closest Case Approach

For this approach, the norm of $IC_{new} - IC_K$ was minimized, where K was the number of known cases from the training set, and these cases were sorted based on the ascending value of the norm, the closest case is the one for which the $norm(IC_{new} - IC_K)$ was the smallest. The velocity field for the new case was approximated as described in Algorithm 1. The Absolute Error (e) for Door Opening experiments at every location for all timesteps is plotted against time in Figure 3.

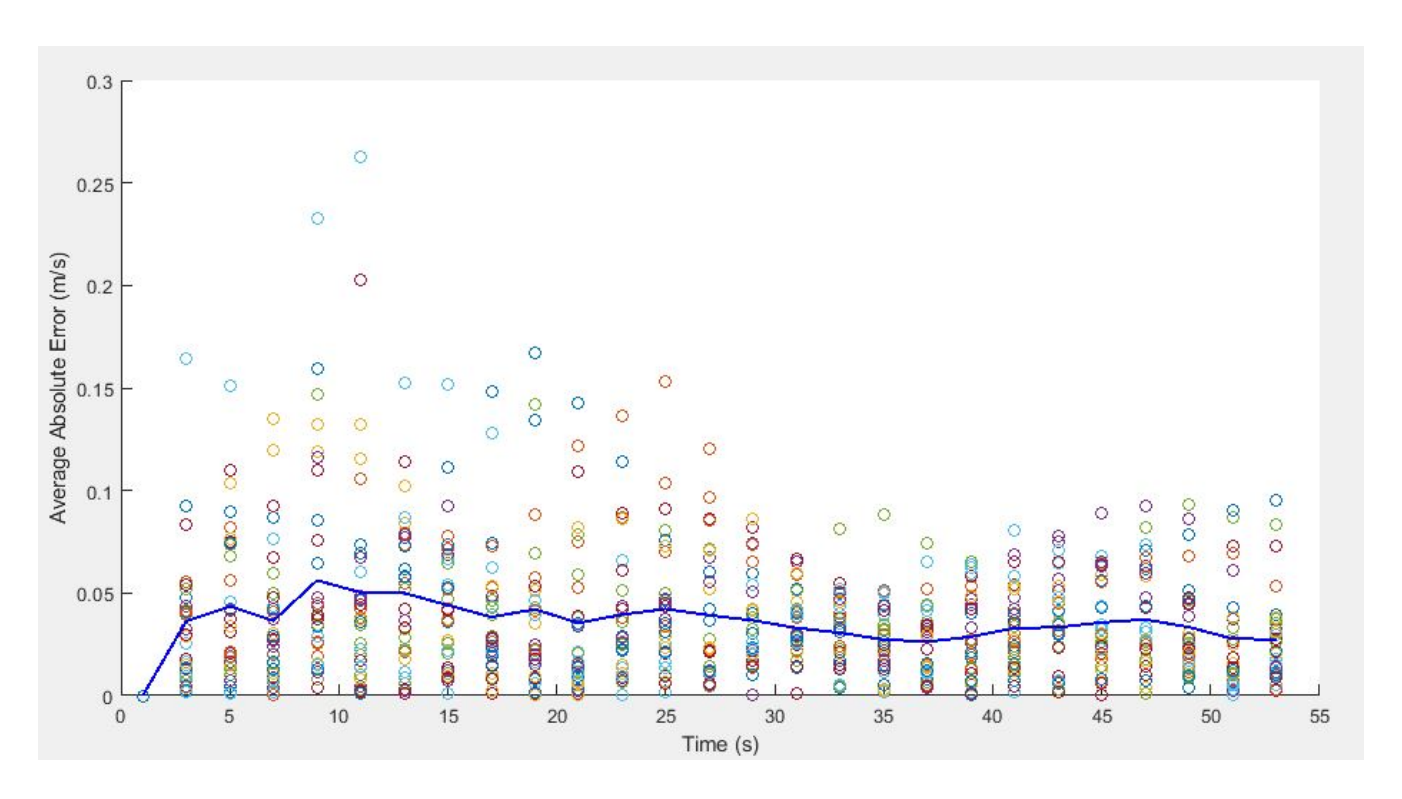


Figure 3: Closest Case Approach - Temporal Trend of Absolute Error: The Pointers Show Absolute Error at All Locations at Every Timestep; The Line Shows Spatially Averaged Absolute Error

From Figure 3, it can be observed that even though for most of the locations the absolute errors are < 0.1 m/s, there are some locations where the errors are higher, specifically until second 30. These locations were found to be either on the proximity of the door's moving edge or locations closed to the wall. Airflow at these locations had turbulent interactions, as the air moving close to the wall, i.e., a stationary boundary, the velocity wakes could not disperse, and hence contributed to the increased error. The distribution of error, visualized in Figure 4, demonstrates it to be a unimodal and symmetric distribution with some outliers in the tails. Fitting a normal distribution to the data, it is observed that the estimated mean of the distribution is very close to zero (0.000105036) (standard error = 0.0016), with an estimated standard deviation of 0.0481215 (standard error = 0.0011.)

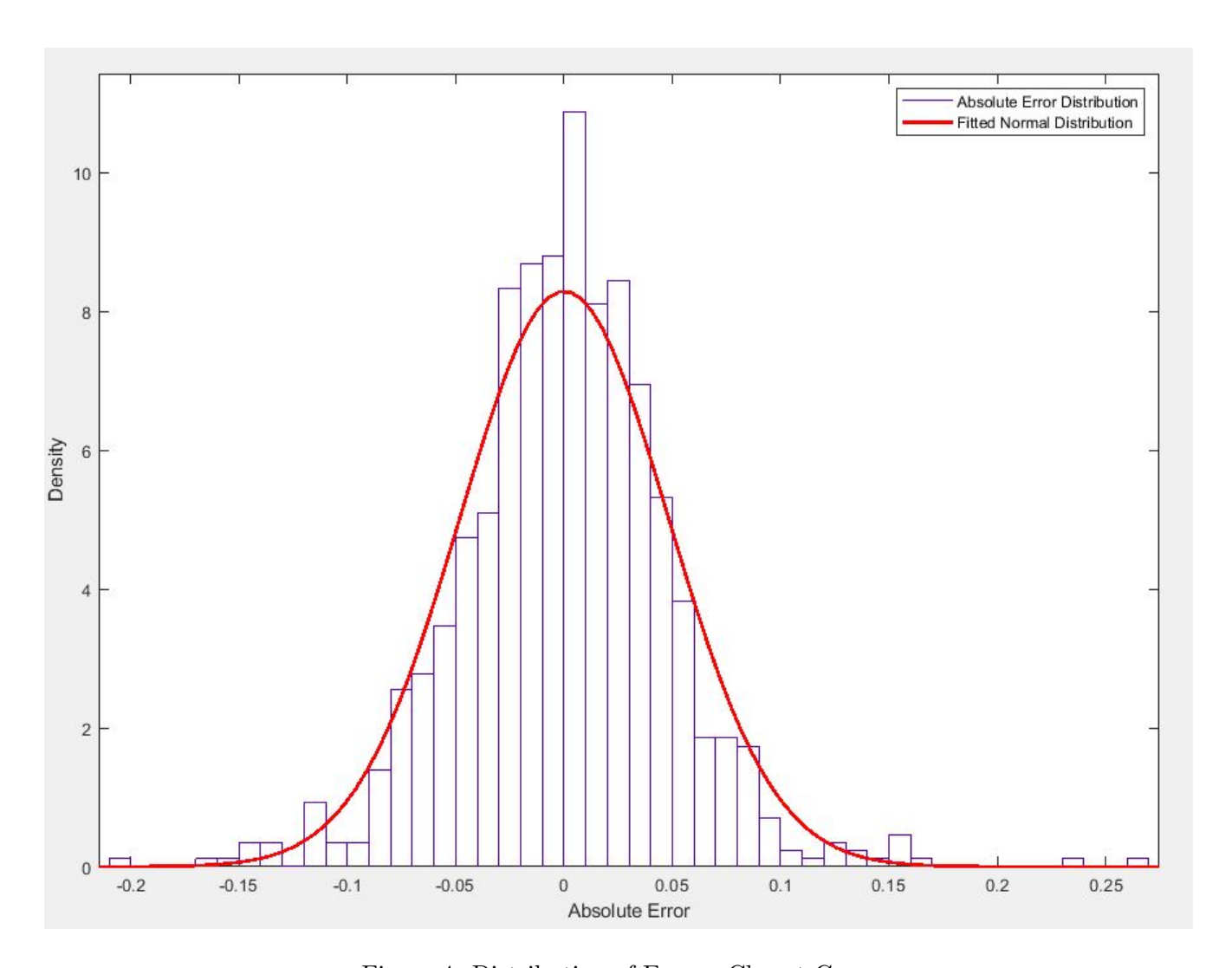


Figure 4: Distribution of Error - Closest Case

Next, instead of calculating α from a single case (whose IC is the closest to the IC of the case that is being predicted), one can use several close cases to approximate α , and in turn, approximate the velocity field for the new case. In this case, α is calculated for each of these selected closed cases, and $\bar{\alpha}$ is calculated by averaging α 's over the number of selected cases, as given in the following equation, where N is the number of close cases selected.

$$\bar{\alpha} = \frac{\sum_{i=1}^{N} \alpha_i}{N} \tag{12}$$

Figure 5 shows the spatially averaged absolute errors for several different values of N. This demonstrates

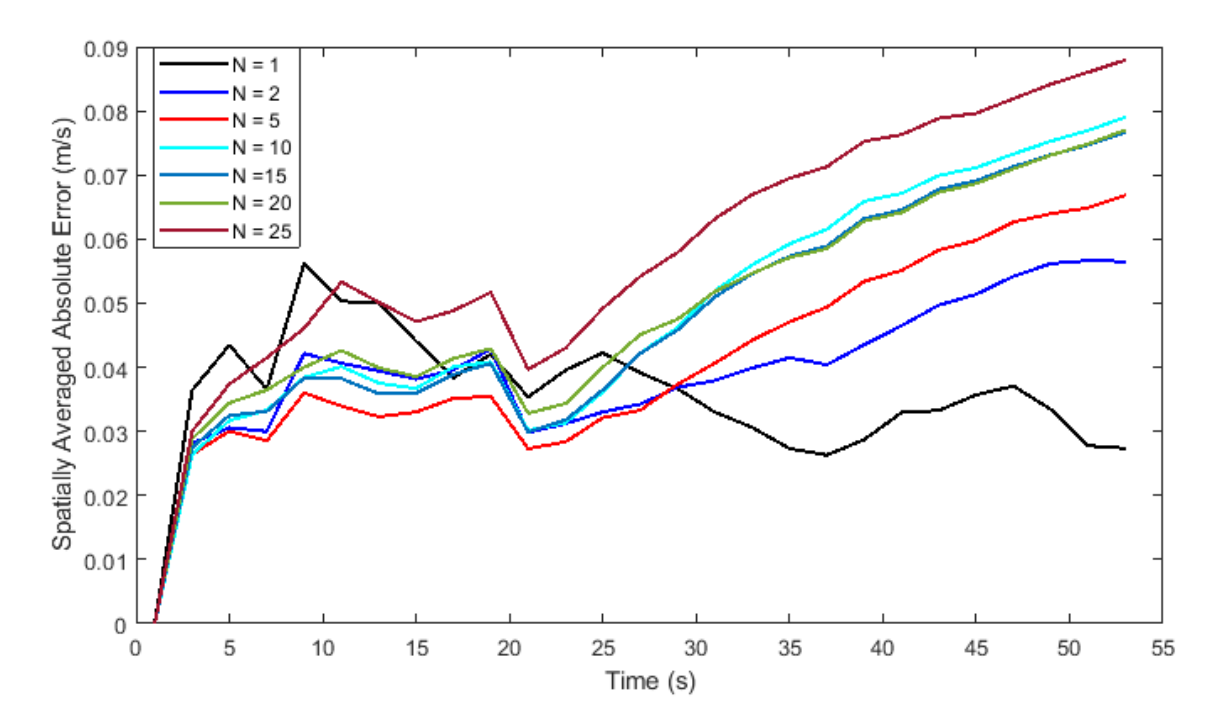


Figure 5: Effect of Number of Close Cases Selected to Approximate α on Average Absolute Error - Closest Case Approach

that the area under the spatially averaged absolute error curve, or overall error, is minimum when N = 1, i.e., the new case is approximated based on the single case whose initial condition was the most similar to the predicted case. For some timesteps, selecting more than one close case may have produced smaller error, but that trend was temporally not consistent - when N > 1, the absolute error tends to increase quickly after 20 seconds. In other words, approximating a new case using only the closest case resulted in less error. Theoretically, this make sense as adding training points that are farther from the test case can create noise in the approximation algorithm.

5.2.3 Dynamic closest Case

For this approach, at the first timestep, the norm of $IC_{new} - IC_K$ was minimized, where K was the number of known cases from the training dataset, and the these cases were sorted based on the ascending value of the norm. For the closest case, i.e., for which the $norm(IC_{new} - IC_K)$ was the smallest, α was calculated using Eq. 6, stored, and used to approximate the velocity vector at the second timestep of the new case (using Algorithm 1). This procedure is done at every timestep n, using the velocity vector at timestep n-1 as the initial condition. As stated earlier, reconstructing α at every timestep can potentially improve the accuracy of approximation, contingent on the training dataset richness. It turned out that

our experimental dataset was not rich enough to accommodate such improvements. That is the closest case solely based on the initial condition remained the closest case throughout the simulation period (i.e.,converging to the Closest Case approach). However, to capture whether this dynamic approach produced any improvements, we changes the number of closest case to N = 2. It can be seen from Figure 6 that the dynamic closest case results in a better approximation of the new case. If the overall spatially averaged error (\bar{E}_{ov}) is described as the area under the curve, then it can be expressed as

$$\bar{E}_{ov} = \int \bar{E} \, dt \tag{13}$$

where \bar{E} is spatially averaged absolute error at each timestep. The overall error (\bar{E}_{ov}) for the dynamic closest case approach is 14% less than the \bar{E}_{ov} computed using the closest case approach. It is also evident from the fact that the \bar{E}_{ov} of the closest case approach starts increasing from second 20, whereas the \bar{E}_{ov} of the dynamic closest case approach starts to blow up from second 33. Within second 30 to second 53, the \bar{E}_{ov} resulted from the dynamic closest case is 36% less than that of \bar{E}_{ov} from the closest case, on average. These observations indicate that using the dynamic closest approach not only approximated the new case more accurately, the transition from the transient event to the steady-state was also faster compared to the closest case approach.

6 Conclusions

In this paper, we have presented a novel methodology called event-based modeling (EBM) to approximate airflow velocities for human-environment interactions such as door opening and walking movements. In this study, real-time experimental data collected at a controlled environment chamber was used to characterize airflow characteristics under occupant movements in a steady-state flow. Data for the changes in flow velocity was collected at several spatial locations, at different heights, for the duration from the start of the intervention until the effects of transient occupant interventions diminished and steady-state conditions were restored. The results presented in this study considered constant boundary conditions. The principal idea behind this study was that the current ventilation system design paradigm does not consider the transient events like occupant introduced perturbations while determining the ventilation requirements and parameters, principally because experimental measurement of the transient events are not feasible, and simulating transient events are time-consuming, and computationally intensive. In response,

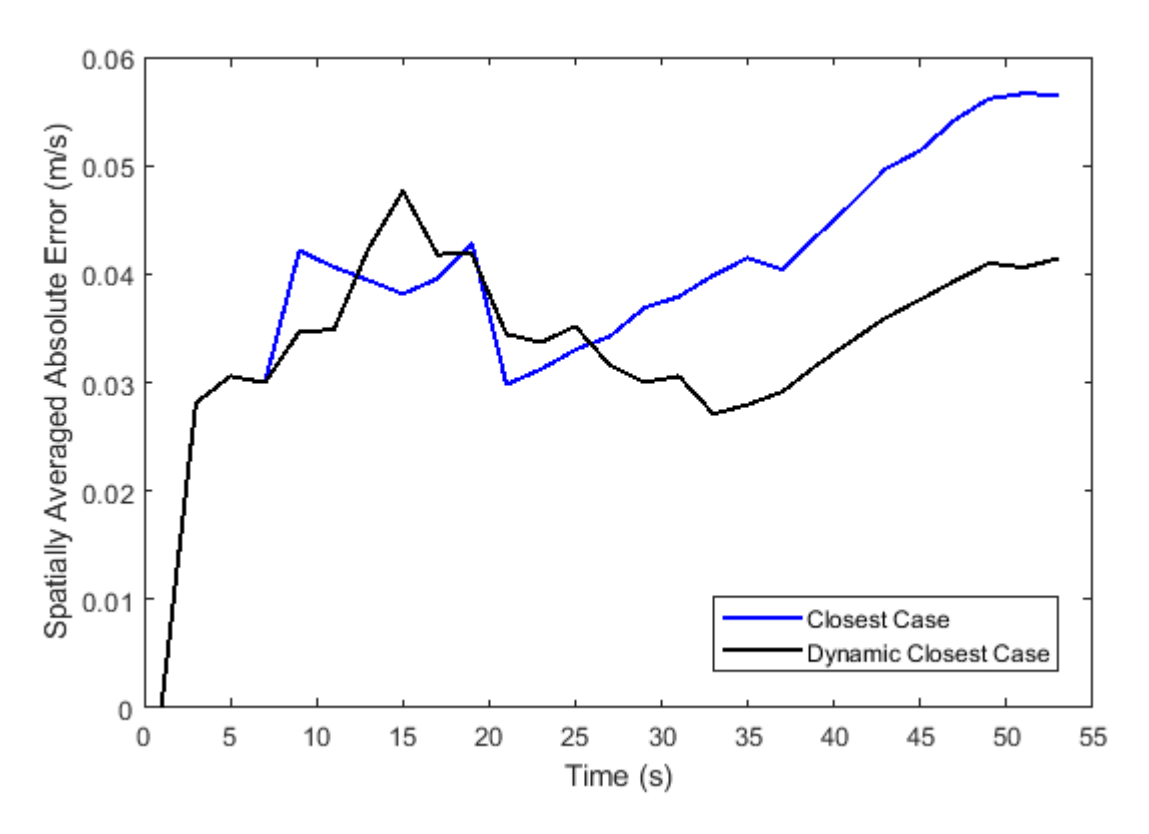


Figure 6: Comparison of Dynamic Closest Case Approach and Closest Case Approach for Approximating a New Case Using Two Closest Cases (N=2) from the Training Dataset

the method presented in this paper can approximate the flow properties under transient events using a data-driven model. If a database of flow properties, either from experimental studies or fluid dynamic simulation can be amassed, EBM can predict the resultant flow characteristics in those environments for separate initial conditions, without having to run another set of experiments or a set of simulations.

The flow velocity was measured at every timestep through experiments. The collected data for all different experimental setups were combined in matrices. To study the efficacy of the proposed EBM model, the aggregated database was divided into a training set and a test set. The training set, containing randomly chosen 80% of the total dataset, was used to calculate identifiers (α 's) that connect the velocity profile at one timestep (m) to the next(m + 1). The test set was made up of the rest 20% of the total data, to compare the approximated velocity field of the new case and one of the measured case. Three methods of combining the the α 's to create the α_{new} have been discussed in this manuscript - namely the weighted average case, closest case, and dynamic closest case. It was shown that the dynamic closest case approach provides the most accurate approximation. The accuracy of the approximation was found through an error index that quantified the difference between the approximated case and a test case.

The weighted average approach was the least effective method of approximating the velocity fields from the known set of cases. The idea behind the weighted average method was that all of the identifiers calculated using the database for training, contributed to the reconstruction of the α_{new} . The contributions of each of the α 's from the training set were calculated in terms of linear coefficients, with a constraint that their sum was equal to one, by comparing the initial condition of all the cases in the training dataset to the initial condition of the new case. This linear combination of the information from the training data was under serious question since the calculation of the identifiers were done using a pseudo-inverse method. The results suggested that the highest error, when spatially averaged, calculated using this weighted average approach, was more than 30% for events with two consecutive interventions.

The closest case approach produced better results when approximating the new case based on the available data. In this approach, the initial condition of the new case is compared to the initial conditions, i.e, the velocity vector at the first timestep, to find out the which case in the training set best represented the initial condition of the new case. The identifiers (α 's) for that case are then used to calculate the velocity vectors for the new case at every timestep. The spatially averaged error for the closest case approach was found to be below 6% over time. Moreover, the error metric was found to be normally distributed. instead of basing the calculation on just one single closest case, the authors also investigated the outcome when several close cases were considered for approximation. Turned out, basing the calculation off of the closest single case produced the least overall error.

In the dynamic closest case approach, the approximation of the new case was calculated dynamically, as the name suggests. Instead of comparing just the initial condition of the new case with the training dataset to find the closest case, in this approach, the velocity vectors calculated at every timestep were compared to the training set and the closest case was found. Ideally, the closest case at every timestep can change, representing the closest flow condition in the chamber at that instant. Interestingly, it was found out that when the approximation was based on the single closest case, the closest case did not change from time to time - essentially converging the calculation to the closest case approach. It was postulated that the limited number of available cases in the training set might have been the reason for the closest case to remain same through all the timesteps. But when the information from more than a single case was used to approximate the new case, dynamic closest approach resulted in a better prediction accuracy throughout the duration, measured using overall spatially averaged error. Lastly, it is critical for successful approximation of a transient event to converge to the steady state condition. This feature was clearly observed in experimental data that the velocity magnitudes converge to the steady

state values approximately in roughly 30 seconds. The dynamic approach satisfies this feature as the absolute errors diminished with time.

7 Limitations and Future Outlook

The experimental method of data collection posed several constraints for this study, specifically because the restricted access to the test chamber and availability of adequate sensing devices. The test chamber was available for a limited time, hence the velocity values could be collected for three initial conditions, i.e., the supply air rates. Additionally, availability of eight sets of omnidirectional velocity sensors at a time led to conducting experiments in sets. Despite these constraints in the experimental procedure at least 30 sets of data was collected for each experiment setup. Even then, to maximize the velocity information over a large spatial area, the sensors were arranged in a sparse way inside the chamber, leaving a significant area of the room where data collection was not possible.

The limited number of spatial locations where data could be collected, led to a comparably smaller dataset. The fact that the dynamic closest case approached converged to the closest case approach, i.e., the closest case did not change from one timestep to another, could be attributed to the unavailability of enough data in the training set that represent the velocity field in that timestep, so the algorithm brought back to the initial closest case for every timestep. Thus, to efficiently implement the EBM model, it is crucial to have a database containing information of a substantial number of cases. Scientists studying the indoor airflow patterns originating from occupant-environment interaction will be able to contribute to building the database. Additionally, Computation Fluid Dynamics (CFD) models can also be an effective source to collect such spatiotemporal velocity information indoors. In the near future, the principle direction of this research is to employ these methodologies for a database that contains the velocity field information from several different initial conditions.

With significant improvements in the database, this EBM method can be very useful to determine the airflow velocity under a transient discrete event like occupant movement. When the airflow velocity is approximated using this data-driven technique, using the Lagrangian framework of particle flow as shown in Eq. 1 can be solved rather easily, considering it an ODE at that point. This way, the dispersion of airborne particles can be approximated under occupant-induced disturbances in a steady state flow environment which offers promise to significant improvement in occupant-centric adaptable ventilation

system design, that can reduce energy use and control contamination dispersion.

References

- [1] S. Brown, M. R. Sim, M. J. Abramson, and C. N. Gray, "Concentrations of volatile organic compounds in indoor air—a review," *Indoor air*, vol. 4, no. 2, pp. 123–134, 1994.
- [2] T. L. Thatcher, T. E. McKone, W. J. Fisk, M. D. Sohn, W. W. Delp, W. J. Riley, and R. G. Sextro, "Factors affecting the concentration of outdoor particles indoors (copi): Identification of data needs and existing data," tech. rep., Lawrence Berkeley National Lab.(LBNL), Berkeley, CA (United States), 2001.
- [3] J. Sundell, H. Levin, W. W. Nazaroff, W. S. Cain, W. J. Fisk, D. T. Grimsrud, F. Gyntelberg, Y. Li, A. Persily, A. Pickering, et al., "Ventilation rates and health: multidisciplinary review of the scientific literature," *Indoor air*, vol. 21, no. 3, pp. 191–204, 2011.
- [4] C.-G. Bornehag, J. Sundell, L. Hägerhed-Engman, and T. Sigsgaard, "Association between ventilation rates in 390 swedish homes and allergic symptoms in children," *Indoor air*, vol. 15, no. 4, pp. 275–280, 2005.
- [5] L. Morawska and J. Cao, "Airborne transmission of sars-cov-2: The world should face the reality," Environment International, p. 105730, 2020.
- [6] Y. Bai, L. Yao, T. Wei, F. Tian, D.-Y. Jin, L. Chen, and M. Wang, "Presumed asymptomatic carrier transmission of covid-19," *Jama*, vol. 323, no. 14, pp. 1406–1407, 2020.
- [7] L. Setti, F. Passarini, G. De Gennaro, P. Barbieri, M. G. Perrone, M. Borelli, J. Palmisani, A. Di Gilio, P. Piscitelli, and A. Miani, "Airborne transmission route of covid-19: why 2 meters/6 feet of inter-personal distance could not be enough," 2020.
- [8] G. Emenius, M. Svartengren, J. Korsgard, L. Nordvall, G. Pershagen, and M. Wickman, "Building characteristics, indoor air quality and recurrent wheezing in very young children—a nested case-control study within the bamse birth cohort," *Indoor Air*.

- [9] D. Norbäck, E. Björnsson, C. Janson, J. Widström, and G. Boman, "Asthmatic symptoms and volatile organic compounds, formaldehyde, and carbon dioxide in dwellings.," Occupational and environmental medicine, vol. 52, no. 6, pp. 388–395, 1995.
- [10] L. Øie, P. Nafstad, G. Botten, P. Magnus, and J. J. Jaakkola, "Ventilation in homes and bronchial obstruction in young children," *Epidemiology*, pp. 294–299, 1999.
- [11] D. Milton, P. Glencross, and M. Walters, "Illness related work absence associated with workplace ventilation and humidification," American Journal of Respiratory Critical Care Medicine, vol. 157, p. A647, 1998.
- [12] A. Bhattacharya, A. R. Metcalf, A. M. Nafchi, and E. S. Mousavi, "Particle dispersion in a cleanroom–effects of pressurization, door opening and traffic flow," *Building Research & Information*, pp. 1–14, 2020.
- [13] A. Bhattacharya, A. Ghahramani, and E. Mousavi, "The effect of door opening on air-mixing in a positively pressurized room: implications for operating room air management during the COVID outbreak," *Journal of Building Engineering*, p. 102900, 2021.
- [14] A. Bhattacharya, J. Pantelic, A. Ghahramani, and E. S. Mousavi, "Three-dimensional analysis of the effect of human movement on indoor airflow patterns," *Indoor air*, vol. 31, no. 2, pp. 587–601, 2021.
- [15] A. Josephson and M. E. Gombert, "Airborne transmission of nosocomial varicella from localized zoster," The Journal of infectious diseases, vol. 158, no. 1, pp. 238–241, 1988.
- [16] Y.-C. Shih, C.-C. Chiu, and O. Wang, "Dynamic airflow simulation within an isolation room," Building and environment, vol. 42, no. 9, pp. 3194–3209, 2007.
- [17] E. S. Mousavi and K. R. Grosskopf, "Airflow patterns due to door motion and pressurization in hospital isolation rooms," Science and Technology for the Built Environment, vol. 22, no. 4, pp. 379– 384, 2016.
- [18] Y.-C. Tung, Y.-C. Shih, and S.-C. Hu, "Numerical study on the dispersion of airborne contaminants from an isolation room in the case of door opening," *Applied Thermal Engineering*, vol. 29, no. 8-9, pp. 1544–1551, 2009.

- [19] N. Gustavsson, "Dispersion of small particles into operating rooms due to door openings," 2010.
- [20] N. J. Adams, D. L. Johnson, and R. A. Lynch, "The effect of pressure differential and care provider movement on airborne infectious isolation room containment effectiveness," American journal of infection control, vol. 39, no. 2, pp. 91–97, 2011.
- [21] R. J. Lynch, M. J. Englesbe, L. Sturm, A. Bitar, K. Budhiraj, S. Kolla, Y. Polyachenko, M. G. Duck, and D. A. Campbell Jr, "Measurement of foot traffic in the operating room: implications for infection control," *American Journal of Medical Quality*, vol. 24, no. 1, pp. 45–52, 2009.
- [22] E. S. Mousavi, R. Jafarifiroozabadi, S. Bayramzadeh, A. Joseph, and D. San, "An observational study of door motion in operating rooms," *Building and Environment*, vol. 144, pp. 502–507, 2018.
- [23] O. Ahmed, J. Mitchell, and S. Klein, "3713 dynamics of laboratory pressurization," ASHRAE Transactions-American Society of Heating Refrigerating Airconditioning Engin, vol. 99, no. 2, pp. 223–229, 1993.
- [24] C. Balocco, G. Petrone, and G. Cammarata, "Assessing the effects of sliding doors on an operating theatre climate," in *Building Simulation*, vol. 5, pp. 73–83, Springer, 2012.
- [25] D. T. Hitchings, "Laboratory space pressurization control systems," ASHRAE Journal-American Society of Heating Refrigerating and Airconditioning Engineers, vol. 36, no. 2, pp. 36–40, 1994.
- [26] D. Kiel and D. Wilson, "Combining door swing pumping with density driven flow," ASHRAE Transactions, vol. 95, no. 2, pp. 590–599, 1989.
- [27] E. B. Smith, I. J. Raphael, M. G. Maltenfort, S. Honsawek, K. Dolan, and E. A. Younkins, "The effect of laminar air flow and door openings on operating room contamination," The Journal of arthroplasty, vol. 28, no. 9, pp. 1482–1485, 2013.
- [28] J. Hang, Y. Li, W. Ching, J. Wei, R. Jin, L. Liu, and X. Xie, "Potential airborne transmission between two isolation cubicles through a shared anteroom," *Building and environment*, vol. 89, pp. 264–278, 2015.
- [29] I. Eames, D. Shoaib, C. Klettner, and V. Taban, "Movement of airborne contaminants in a hospital isolation room," *Journal of the Royal Society Interface*, vol. 6, no. suppl_6, pp. S757–S766, 2009.

- [30] A. Hathway, I. Papakonstantis, A. Bruce-Konuah, and W. Brevis, "Experimental and modelling investigations of air exchange and infection transfer due to hinged-door motion in office and hospital settings," *International Journal of Ventilation*, vol. 14, no. 2, pp. 127–140, 2015.
- [31] J. Villafruela, J. San José, F. Castro, and A. Zarzuelo, "Airflow patterns through a sliding door during opening and foot traffic in operating rooms," *Building and Environment*, vol. 109, pp. 190– 198, 2016.
- [32] Z. Lin, T. Chow, and C. Tsang, "Effect of door opening on the performance of displacement ventilation in a typical office building," *Building and Environment*, vol. 42, no. 3, pp. 1335–1347, 2007.
- [33] I. G. Papakonstantis, E. A. Hathway, and W. Brevis, "An experimental study of the flow induced by the motion of a hinged door separating two rooms," *Building and Environment*, vol. 131, pp. 220–230, 2018.
- [34] A. Bhattacharya and E. Mousavi, "The effect of boundary conditions on transient airflow patterns: A numerical investigation of door operation," ASHRAE Transactions, vol. 126, pp. 239–246, 2020.
- [35] J. M. Leclair, J. A. Zaia, M. J. Levin, R. G. Congdon, and D. A. Goldmann, "Airborne transmission of chickenpox in a hospital," *New England Journal of Medicine*, vol. 302, no. 8, pp. 450–453, 1980.
- [36] E. BjØrn, M. Mattsson, M. Sandberg, and P. V. Nielsen, "Displacement ventilation: effects of movement and exhalation," 1997.
- [37] M. Mattsson, "Velocity field created by moving objects in rooms," in *Proc. of the 5 ithic International Conference on Air Distribution in Rooms*, 1996, 1996.
- [38] P. V. Nielsen, "The importance of a thermal manikin as source and obstacle in full-scale experiments," 1999.
- [39] S. B. Poussou, S. Mazumdar, M. W. Plesniak, P. E. Sojka, and Q. Chen, "Flow and contaminant transport in an airliner cabin induced by a moving body: Model experiments and cfd predictions," *Atmospheric Environment*, vol. 44, no. 24, pp. 2830–2839, 2010.
- [40] N. Luo, W. Weng, X. Xu, and M. Fu, "Human-walking-induced wake flow-piv experiments and cfd simulations," *Indoor and Built Environment*, vol. 27, no. 8, pp. 1069–1084, 2018.

- [41] S. Mazumdar, Y. Yin, A. Guity, P. Marmion, B. Gulick, and Q. Chen, "Impact of moving objects oncontaminant concentration distributions in an inpatient ward with displacement ventilation," Hvac&R Research, vol. 16, no. 5, pp. 545–563, 2010.
- [42] H. Brohus, K. Balling, and D. Jeppesen, "Influence of movements on contaminant transport in an operating room.," *Indoor air*, vol. 16, no. 5, pp. 356–372, 2006.
- [43] Z. Han, W. Weng, Q. Huang, M. Fu, J. Yang, and N. Luo, "Aerodynamic characteristics of human movement behaviours in full-scale environment: comparison of limbs pendulum and body motion," *Indoor and Built Environment*, vol. 24, no. 1, pp. 87–100, 2015.
- [44] Y. Wu and N. Gao, "The dynamics of the body motion induced wake flow and its effects on the contaminant dispersion," *Building and environment*, vol. 82, pp. 63–74, 2014.
- [45] O. Rouaud, M. Havet, and C. Solliec, "Influence of external perturbations on a minienvironment: experimental investigations," *Building and Environment*, vol. 39, no. 7, pp. 863–872, 2004.
- [46] Y. Cheng and Z. Lin, "Experimental investigation into the interaction between the human body and room airflow and its effect on thermal comfort under stratum ventilation," *Indoor air*, vol. 26, no. 2, pp. 274–285, 2016.
- [47] J.-I. Choi and J. R. Edwards, "Large-eddy simulation of human-induced contaminant transport in room compartments," *Indoor air*, vol. 22, no. 1, pp. 77–87, 2012.
- [48] Y. Tao, K. Inthavong, and J. Tu, "Experimental and cfd modelling of indoor air and wake flow from a moving manikin," *Indoor Built Environ*, vol. 26, pp. 185–198, 2017.
- [49] J. Hang, Y. Li, and R. Jin, "The influence of human walking on the flow and airborne transmission in a six-bed isolation room: tracer gas simulation," *Building and Environment*, vol. 77, pp. 119–134, 2014.
- [50] A. C. Lai and W. W. Nazaroff, "Modeling indoor particle deposition from turbulent flow onto smooth surfaces," *Journal of aerosol science*, vol. 31, no. 4, pp. 463–476, 2000.
- [51] S. Apte, K. Mahesh, and T. Lundgren, "A eulerlan-lagrangian model to simulate two-phase/particulate flows," tech. rep., MINNESOTA UNIV MINNEAPOLIS, 2003.

- [52] Z. Zhang and Q. Chen, "Prediction of particle deposition onto indoor surfaces by cfd with a modified lagrangian method," *Atmospheric Environment*, vol. 43, no. 2, pp. 319–328, 2009.
- [53] W. C. Hinds, Aerosol technology: properties, behavior, and measurement of airborne particles. John Wiley & Sons, 1999.
- [54] F. Memarzadeh, "The environment of care and health care associated infections—an engineering perspective," American Society of Healthcare Engineering of the American Hospital Association, 2011.
- [55] R. Carneiro, P. D. Gaspar, and P. D. d. Silva, "3d and transient numerical modelling of door opening and closing processes and its influence on thermal performance of cold rooms," Applied Thermal Engineering, vol. 113, pp. 585–600, 2017.
- [56] N. Li and Q. Chen, "Study on dynamic thermal performance and optimization of hybrid systems with capillary mat cooling and displacement ventilation," *International Journal of Refrigeration*, vol. 110, pp. 196–207, 2020.
- [57] X. Du, B. Li, H. Liu, Y. Wu, and T. Cheng, "The appropriate airflow rate for a nozzle in commercial aircraft cabins based on thermal comfort experiments," *Building and Environment*, vol. 112, pp. 132– 143, 2017.
- [58] Y. Wu, H. Liu, B. Li, Y. Cheng, D. Tan, and Z. Fang, "Thermal comfort criteria for personal air supply in aircraft cabins in winter," *Building and Environment*, vol. 125, pp. 373–382, 2017.
- [59] M. Jaszczur, P. Madejski, S. Kleszcz, M. Zych, and P. Palej, "Numerical and experimental analysis of the air stream generated by square ceiling diffusers," in E3S Web of Conferences, vol. 128, p. 08003, EDP Sciences, 2019.
- [60] M. Borowski, M. Jaszczur, D. Satoła, and M. Karch, "Air flow characteristics of a room with air vortex diffuser," in MATEC Web of Conferences, vol. 240, p. 02002, EDP Sciences, 2018.

Conflict of Interest (Please upload in Word format)

Declaration of interests

☐The authors declare that they have no known competing financial interests or personal relationships that could have appeared to influence the work reported in this paper.

⊠The authors declare the following financial interests/personal relationships which may be considered as potential competing interests:

Ehsan Mousavi reports financial support was provided by National Science Foundation.